**IEEE** *Access*

## RESEARCH ARTICLE

# Configuration Design and Gait Analysis of Wheel-Legged Mobile Robot Based on the Rubik's Cube Mechanism

**WENJUAN LU[1], JIAHAO ZENG[2], SHIHAO DONG[2], DABAO FAN[2], YA LIU[2], DAXING ZENG[1], AND MIAOYAN CAO[2]**
[1]DGUT Innovation Center of Robotics and Intelligent Equipment, Dongguan 523808, China
[2]School of Mechanical Engineering, Yanshan University, Qinhuangdao 066004, China

Corresponding author: Daxing Zeng (zengdx@dgut.edu.cn)

**ABSTRACT** Traditional mobile robots have limitations in obstacle-crossing ability, motion stability and load-bearing capacity in complex environments, which make them difficult to be applied on a large scale. Based on the Rubik's Cube mechanism (RCM) with strong coupling and variable topology, a polymorphous wheel-legged mobile robot (WLMR) is proposed. Aiming at the problems of the classical three-order RCM, such as small internal space, difficult processing and demanding precision, a new type of chute third-order RCM is designed, and its mechanical characteristics analysis and feasibility analysis are carried out. What's more, a driving configuration analysis method is established according to different driving configuration relationships, and the configuration of WLMR is determined by the configuration stability analysis. Then, a WLMR with polymorphism is designed, and gait planning and gait stability analysis are conducted. Eventually, the co-simulation and prototype experiments are performed to verify the efficiency of the WLMR's straight motion, in-situ rotation, obstacle-crossing and morphology transformation in complex environments. This research not only provides a reference for the design of polymorphous mobile robots, but also opens up ideas for the application of the RCM in daily production and life.

**INDEX TERMS** Rubik's Cube mechanism, mobile robot, polymorphism, configuration design, gait analysis.

## I. INTRODUCTION

As an important field of robotics research, mobile robots integrate multiple functions such as visual recognition, trajectory planning, and mobile obstacle-crossing. They have not only been widely used in daily life, but also played an important role in the fields of aerospace exploration, military reconnaissance, rescue and disaster relief, and transportation of dangerous objects [1]. According to the movement mode, the existing mobile robots are mainly divided into the following

The associate editor coordinating the review of this manuscript and approving it for publication was Wai-Keung Fung.

four types: wheeled robots, legged robot, crawler robots and wheel-legged robots. Among them, wheel-legged mobile robots (WLMRs) [2], [3] combine the advantages of wheeled robots and legged robots, which can not only move quickly on flat or soft ground, but also cross obstacles on complex unstructured ground. With the increasing complexity of the environment and terrain, WLMR have also become the focus of research by many scholars at home and abroad.

There are three basic types of the existing WLMRs: wheel-leg coordination type, wheel-leg shape independent type, and wheel-leg structure variable type. (1) Wheel-leg coordination type: This type of mobile robot mainly moves by

virtue of the coordinated action of wheels and legs. The wheels are generally small, and the wheel-leg shape conversion can be realized by locking the wheels. For example, Bjelonic et al [4] developed a quadruped robot, which is equipped with four non-steerable and torque-controlled wheels on four legs; Morihiro *et al.* [5] proposed a WLMR composed of six open-chain mechanisms; Chen *et al.* [6], [7] developed an electric parallel hexapod robot based on the Stewart platform. (2) Wheel-leg shape independent type: This type of mobile robot can transform its shape to adapt to different terrains according to needs. For example, Nakajima *et al.* [8] developed a robot with two large wheels and four legs; Zhang *et al.* [9] put the wheels on the mechanical legs of the robot, and proposed a hexapod wheel-leg compound robot that can switch multiple operation modes. (3) Wheel-leg structure variable type: This type of mobile robot can change the structure of the wheel part to turn the wheels into mechanical legs. For example, Taiwan University has proposed two transformable wheel-legged robots, Quattroped [10] and TurboQuad [11]; The deformable wheel proposed by Zhou *et al.* [12] will use the internal spokes to convert the entire wheel frame into feet when encountering obstacles, so as to realize the wheel-leg shape conversion of the robot.

To sum up, WLMRs have been extensively explored, which have greatly promoted the development of theoretical research and application promotion of wheel-legged robot. However, mobile robots still have certain limitations in obstacle-crossing ability, motion stability, and load-bearing capacity, especially their weak adaptive ability when dealing with complex environments. Most of them cannot be applied to the differentiated terrain in the environment at the same time, which limits the large-scale application of WLMRs.

In order to improve the adaptability of robots to different terrains, many scholars have introduced the concept of metamorphosis into the research of mobile robots based on the characteristics that metamorphic mechanisms can generate new configurations through merging, separation or geometric singularity. For example, Dai *et al.* [13] launched the metamorphic dexterous hand for the first time in the world, and used it in the waist structure of the crawling robot to develop a metamorphic robot that can adapt to different environments; Zhen *et al.* [14] proposed a new type of quadrupedal metamorphic crawling robot, which can meet the requirements of movement in different terranes through the combination of waist activity and gait; Liu *et al.* [15] developed a deformable wheel-legged robot based on a single-loop closed-chain 2RP3R metamorphic mechanism, which can realize the conversion between wheel-leg shapes by using its single-loop closed-chain metamorphic mechanism. Although some progress has been made in the research on mobile metamorphic robots, the study on multi-configuration and highly adaptable mobile robots is still in the ascendant, and there is still a gap between most robots and practical application requirements.
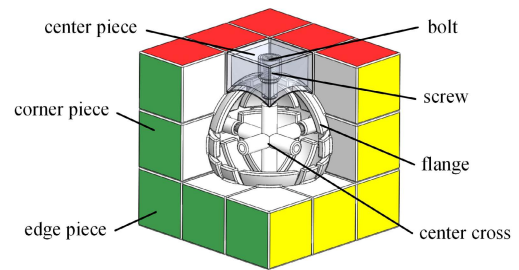


**FIGURE 1.** The structure of the classic third-order RCM.

As a metamorphic mechanism with strong coupling and variable topology, the Rubik's Cube has hundreds of millions of states [17]. In view of the characteristics of free combination of sub-pieces of Rubik's Cube mechanism (RCM) [18], it is applied to the field of mobile robots. The mobile robot combined with the RCM can carry out corresponding shape transformation and adaptive adjustment in different occasions, which can greatly improve its mobile operation ability in various complex environments. Based on this, a new third-order RCM and driving configuration analysis method are proposed, which is introduced into the design of mobile robots to carry out the research of WLMRs based on RCM. It mainly includes: designing a new chute third-order RCM, optimizing the four-drive number configuration through the analysis of driving configuration, and applying it to the wheel-leg conversion module; Furthermore, a WLMR with multiple forms is proposed, and gait planning and gait stability analysis of the robot are carried out; The motion feasibility of the mobile robot in complex environments is verified through co-simulation and prototype experiments.

## II. DESIGN AND ANALYSIS OF NEW CHUTE RCM
### A. THE DESIGN OF THE CHUTE THIRD-ORDER RCM
The classic third-order RCM is shown in Fig. 1. It is mainly composed of 12 edge pieces, eight corner pieces, six center pieces, six bolts, six springs and one center cross. The center piece is pressed inward by screws and springs. There are flanges inside the edge piece and corner piece. the center piece is inward against the corner pieces and edge pieces of the corresponding layer, and all the sub-pieces of the Rubik's Cube are interlocked.

When the RCM is in the non-orthogonal state [19], all sub-pieces on the rotating layer are regarded as a component, which forms a revolute pair with the central cross, and there is only one rotational degree of freedom at this time; In the orthogonal state, each sub-piece belongs to multiple rotating layers, and all sub-pieces can rotate around the common ball pair with three rotational degrees of freedom.

Due to the existence of the flange of the arc surface, the classic third-order RCM has problems such as small internal space, difficult processing, and strict precision requirements. Based on this, a new type of chute three-order RCM is proposed, as shown in Fig. 2.
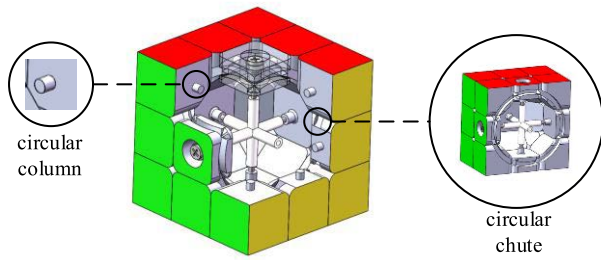
**FIGURE 2.** The structure of the chute third-order RCM.

The positioning structure between the sub-pieces of the chute third-order RCM is changed from the internal flange structure to the chute structure, and cylindrical columns are set on the three sides of the corner piece. The contact surface between each edge piece and the corner piece is provided with a chute, and the contact surface between the edge piece and the center piece is provided with columns. The four contact surfaces between the center piece and the adjacent corner pieces are provided with chutes to meet the rotation requirements of the corresponding layer.

Compared with the way that all the sub-pieces in the classic RCM move in the same spherical orbit formed by the flange, the sub-pieces of each layer of the new RCM move in an independent circular orbit matched with the columns of the corresponding layer. In the non-orthogonal state of the chute RCM, the column can rotate along the circular chute formed by the edge piece and the center piece of the middle layer; In the orthogonal state, the corner pieces and edge pieces of the cube can rotate along the circular chutes in three directions respectively, so as to realize the metamorphic function of rotating each layer of the cube and changing the position of the sub-pieces.

On the basis of realizing the functions of normal rotation and metamorphic transformation, the new chute RCM effectively increases the space inside the Rubik's Cube, reduces the requirement for accuracy, and each sub-piece is easier to process due to the elimination of the complex spherical surface. The overall structure has better mechanical characteristics.

## B. FORCE ANALYSIS OF RCM BEFORE AND AFTER OPTIMIZATION

The force comparison analysis of the third-order RCM before and after the above optimization is carried out, and the force characteristics of the rotating layer in the non-orthogonal state and the force characteristics of each sub-piece in the orthogonal state are respectively studied. The force analysis is shown in Fig. 3 and Fig. 4.

In the non-orthogonal state, the mechanical properties of the mechanism before and after optimization are the same. At this time, the rotating layer can be regarded as a component, which is subjected to the supporting force (($F_{AN}$ in Fig. 3(a) and $F_{AN}'$ in Fig. 4(a)) from the fixed layer and the elastic force (($F_{A0}$ in Fig. 3(a)) and $F_{A0}'$ in Fig. 4(a)) of the spring. The two forces are equal in magnitude and opposite
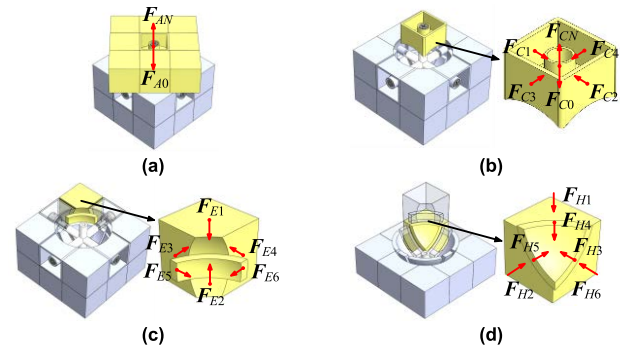


**FIGURE 3.** The force analysis of classical third-order RCM. (a) rotating layer in the non-orthogonal state. (b) center piece in the orthogonal state. (c) edge piece in the orthogonal state. (d) corner piece in the orthogonal state.



**FIGURE 4.** The force analysis of chute third-order RCM. (a) rotating layer in the non-orthogonal state. (b) center piece in the orthogonal state. (c) edge piece in the orthogonal state. (d) corner piece in the orthogonal state.
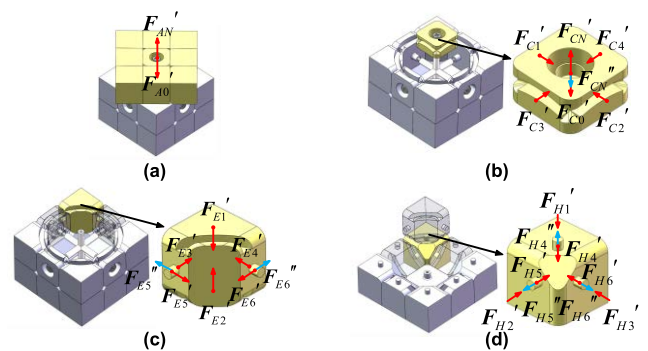
in direction, and the RCM is in equilibrium. The following will analyze the similarities and differences of the mechanical properties of the RCM in the orthogonal state before and after optimization.

(1) Force analysis of classical third-order RCM in the orthogonal state

The force of the center piece of the transfer layer in the orthogonal state of the classical third-order RCM is shown in Fig. 3(b), where $F_{CN}$ is the combined force of the center piece subjected to the support force exerted by the neighboring sub-pieces through the flanges. $F_{C0}$ is the elastic force of the spring. $F_{C1}$, $F_{C2}$, $F_{C3}$ and $F_{C4}$ are the pressures exerted by the adjacent edge piece through the side face, and each force meets Eq. (1).

$$F_{CN} + F_{C0} = 0$$
$$F_{C1} + F_{C2} = 0$$
$$F_{C3} + F_{C4} = 0 \tag{1}$$

The edge pieces are subjected to the pressure exerted on them by the adjacent sub-pieces, as shown in Fig. 3(c), where $F_{E1}$ and $F_{E2}$ are the pressure exerted by the upper and lower corner-cubes through the contact surface. $F_{E3}$ and $F_{E4}$ are the pressures exerted on them by two adjacent center

pieces. $F_{E5}$ and $F_{E6}$ are the pressure exerted by the adjacent center pieces through the flanges, and each force satisfies the Eq. (2).

$$F_{E1} + F_{E2} = 0$$
$$F_{E3} + F_{E4} + F_{E5} + F_{E6} = 0 \quad (2)$$

The corner piece is in contact with three edge pieces, and the forces are shown in Fig. 3(d), where $F_{H1}$, $F_{H2}$ and $F_{H3}$ are the pressures exerted on them by the adjacent edge pieces through the contact surface. $F_{H4}$, $F_{H5}$ and $F_{H6}$ are the pressures exerted on them by the adjacent edge pieces through the flanges, and each force satisfies Eq. (3).

$$F_{H1} + F_{H2} + F_{H3} + F_{H4} + F_{H5} + F_{H6} = 0 \quad (3)$$

(2) Force analysis of chute third-order RCM in the orthogonal state

The chute third-order RCM optimizes the internal flanges structure into a chute structure. The corner-cubes, the edge pieces and the center piece can be mechanically constrained to each other by the columns and the chute, and the center piece is constrained by the spring to move outward. The force analysis of each sub-piece is carried out in the orthogonal state, the center piece of the rotating layer is subjected to the forces shown in Fig. 4(b), where $F_{C1}'$, $F_{C2}'$, $F_{C3}'$, $F_{C4}'$ are the pressures exerted on it by the sides of the adjacent edge pieces, and due to the existence of the chute structure, the center piece is subjected to the pressures $F_{CN}'$ and $F_{CN}''$ in both directions exerted by the adjacent edge piece columns, where $F_{C0}'$ is the elastic force exerted by the spring on it, and each force satisfies the Eq. (4).

$$F_{CN}' + F_{C0}' + F_{CN}'' = 0$$
$$F_{C1}' + F_{C2}' = 0$$
$$F_{C3}' + F_{C4}' = 0 \quad (4)$$

The forces of the edge pieces in the orthogonal state are shown in Fig. 4(c), where $F_{E1}'$, $F_{E2}'$, $F_{E3}'$, $F_{E4}'$ are the pressures exerted on them by the contact surfaces of the adjacent sub-pieces, $F_{E5}'$, $F_{E5}''$, $F_{E6}'$, $F_{E6}''$ are the pressures exerted on them by the adjacent center pieces through the columns, and each force satisfies the Eq. (5).

$$F_{E1}' + F_{E2}' = 0$$
$$F_{E3}' + F_{E4}' + F_{E5}' + F_{E6}' + F_{E5}'' + F_{E6}'' = 0 \quad (5)$$

The force of the corner piece is shown in Fig. 4(d), where $F_{H1}'$, $F_{H2}'$, $F_{H3}'$ are the pressures exerted on it by the contact surface of the adjacent edge pieces, $F_{H4}'$, $F_{H4}''$, $F_{H5}'$, $F_{H5}''$, $F_{H6}'$, $F_{H6}''$ is the pressure exerted on it by the adjacent edge pieces through the column, and each force satisfies the Eq. (6).

$$F_{H1}' + F_{H2}' + F_{H3}' + F_{H4}' + F_{H5}'$$
$$+ F_{H6}' + F_{H4}'' + F_{H5}'' + F_{H6}'' = 0 \quad (6)$$

Analyzing and comparing the similarities and differences of the force characteristics of the third-order RCM before and after the optimization, it is clear that the same is true that both RCMs can maintain the mechanical equilibrium in the orthotropic and non-orthotropic states. Unlike the classical third-order RCM, where adjacent sub-pieces are in lateral contact with each other, and the corner and edge pieces are in contact with the inner spherical surface of the center piece through the flanges. Each corner and edge piece is bound by the adjacent center piece, when all outward forces are acting on the center piece. The chute third-order RCM is mainly constrained by the interaction of the columns and slots between the sub-pieces.

The chute third-order RCM constitutes a constraint relationship different from the traditional RCM in the movement process by optimizing the rotation mode. It achieves the mechanical balance on the basis of alleviating the problems of small internal space, difficult processing and demanding precision requirements of the original structure. The new mechanism not only ensures the metamorphic function for the rotation of each layer of the RCM and the position change of the sub-pieces, but also reduces the influence of the spring elasticity in the movement of the RCM, making the movement more supple.

### C. FEASIBILITY ANALYSIS

Based on the above analysis about the structure and force characteristics of the new chute structure, the classical third-order RCM and the optimized chute third-order RCM are compared in terms of motion mechanism, mechanical characteristics, processing difficulty, precision requirements and internal space. The following analyzes the feasibility of its application in practical production and life.

(1) Motion Mechanism

Although the third-order RCM adopts different rotation structures and constraint forms before and after the optimization, both can realize the exchange of sub-piece positions through the rotation of orthotropic and non-orthotropic states of each layer, so as to realize the morphological transformation and metamorphosis characteristics.

(2) Mechanical Characteristics

The classical third-order RCM mainly generates plane pairs and spherical pairs through the contact between the sub-pieces, so that each corner piece and edge piece is constrained by the adjacent center piece. These restraining forces acting on the center piece are mechanically balanced with the elastic force of spring. The chute third-order RCM is mechanically balanced by the sliding restraints between the columns and chutes of the sub-pieces, which can weaken the influence of the spring force in the movement.

(3) Processing Difficulty

The classical third-order RCM contains many complex-shaped flanges structures in order to form the spherical surface required for sliding. Therefore, the traditional RCM is very difficult to process. The chute third-order RCM eliminates the original spherical surface by using the chute structure, which greatly reduces the processing difficulty.

**TABLE 1.** Comparison of the performance of the RCM before and after optimization.

| Performance | Classic | Chute |
|---|---|---|
| Rotating structure | Corner-spherical surface | Column-chute surface |
| Processing difficulty | High | Low |
| Precision requirements | High | Low |
| Internal space | Small | Big |
| Motion pair in the orthogonal state | Spherical pair | Revolute pair |
| Motion pair in the non-orthogonal state | Revolute pair | Revolute pair |
| Mechanical characteristics | Balanced | Balanced |

**TABLE 2.** Wheel-leg conversion module configuration.

| Driving number | Configuration number |
|---|---|
| 0 | 1 |
| 1 | 6 |
| 2 | 15 |
| 3 | 20 |
| 4 | 15 |
| 5 | 6 |
| 6 | 1 |



**FIGURE 5.** Four-drive number preferred configuration. (a) configuration A. (b) configuration B.

(4) Precision Requirements

As the sub-pieces of the classical third-order RCM need to move under the same spherical pair, the low processing accuracy will make the flange surfaces of each sub-piece not on the same spherical surface. The RCM is prone to stress concentration during the process of rotation, which causes the phenomenon of non-smooth rotation. The sub-pieces of each rotating layer of the chute third-order RCM move in different circular chutes, reducing the number of sub-pieces under the same motion pair, and lowering the requirement for machining accuracy.

(5) Internal Space

The classic third-order RCM has a small internal space due to the existence of internal flanges, which makes it impossible to add motors and control elements inside. In contrast, the chute third-order RCM sets the columns and chutes on the side of the sub-piece, which effectively increases the internal space and provides the possibility to realize the motor drive.

The performance of the RCM before and after optimization is compared, as shown in Table 1.

By optimizing the rotation mode of the RCM, the new mechanism realizes the overall constraint and coordination on the basis of the normal rotation function. Based on the multi-modality, low processing difficulty, low precision requirements, large internal space, and smooth motion of the new chute RCM, it is applied to the field of mobile robots. The design and analysis of WLMR based on RCM are carried out from the aspects of wheel-leg conversion, configuration analysis and gait generation.

## III. ANALYSIS OF DRIVING CONFIGURATION
### A. METAMORPHOSIS PRINCIPLE AND CONFIGURATION SYNTHESIS

Based on the flexible metamorphosis characteristics of RCM, it is used as the wheel-leg conversion module of the mobile robot. A driving motor can be added in the internal space of the RCM to realize the automatic control. Based on the principle that the motor is energized to generate the holding torque, its wheel-leg conversion module can adopt different driving and installation modes to realize configuration conversion.
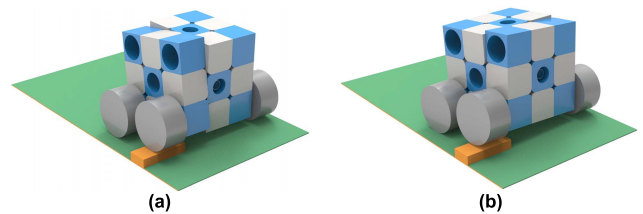
During the rotation of the third-order RCM, the position of the center piece remains unchanged, while each corner piece (edge piece) can move to any position where the corner piece (edge piece) is stored, which makes the number of Rubik's Cube states reach an amazing number.

The number of drives inside the RCM can't exceed six at most. Each drive motor can drive the rotation of one rotating layer or lock the rotation of this layer. Therefore, theoretically, the wheel-leg conversion module has the following 64 configurations, as shown in Table 2.

When the driving number is zero, each rotating layer of the wheel-leg conversion module can rotate under the action of external force. At this time, the wheel-leg conversion configuration is the same as the traditional RCM, and its metamorphic function cannot be realized through active control. When the driving number is six, the mobile robot can realize the wheel-leg conversion function through the active control of the motor. When the motor does not work, each rotating layer of the wheel-leg conversion module is locked by the motor, and the conversion module is equivalent to a whole.

In order to ensure that the mobile robot can not only realize the form conversion function, but also improve the stability through the adaptive rotation of the rotating layer. In this paper, the four-drive configuration is selected as the configuration of the wheel-leg conversion module. Among them, the drive of the upper and lower layer is used to meet the rotation requirements of the upper layer actuator in some special cases, while the two driving of the side layer can be symmetrically arranged to realize the function of form conversion. Finally, two configurations are selected as the prototype of the wheel-leg conversion module of the mobile metamorphic robot, as shown in Fig. 5.

In configuration A, the front, rear, upper and lower rotating layers can be driven by a motor to realize active rotation, the front and rear rotating layers can realize the form conversion, and the left and right rotating layers can self-adaptively rotate to make the four wheels contact the ground when crossing obstacles to improve the stability. On the contrary, the left and right rotating layers and the up and down rotating layers of configuration B are motor driving layers, and the left and right rotating layers can realize the form conversion, while the front and rear rotating layers can rotate adaptively.

## B. CONFIGURATIONAL STABILITY ANALYSIS

The stability of a robot is the ability to resist tipping under various conditions, and its stability is an extremely important index during the movement of a mobile robot. If the stability of the mobile robot is poor, it will easily tip over in the process of movement or morphology transformation, which will lead to a series of problems such as structural damage, driving grounding and control disconnection.

The stability pyramid technique [19] is used to analyze and compare the obstacle-crossing stability of the robot in wheeled form, so as to determine the appropriate wheel-leg conversion module configuration. When the front, rear, left and right rotating layers of wheel-leg conversion module are controlled by the motor, the robot can't adaptively rotate the four rotating layers when crossing obstacles. At this time, the robot configuration is equivalent to a whole, which is taken as the control group for configuration stability analysis and defined as configuration C.

Stability pyramid are established for the three configurations in turn, as shown in Fig. 6, where $p_g$ is the centroid of the robot, and the coordinate system is established with $p_g$ as the origin. Among them, the forward direction of the robot is the positive direction of X-axis, the positive direction of Y-axis on the right and the positive direction of Z-axis on the top, and $p_n(n = 1\text{-}4)$ is the contact point between the wheel and the ground. The stability pyramid is formed by taking $p_g$ as the stability pyramid apex and $p_n$ as the bottom corner.

For the convenience of calculation, the wheel-leg conversion module of robot is regarded as a cube, with each cube edge length of 30mm and the wheel diameter of 48mm. The edge line at the bottom of the stability pyramid is called the tipping edge line and is denoted as $a_i$ ($i = 1, \ldots$, n), and its calculation equation is as Eq. (7).

$$a_i = \mathbf{p}_{i+1} - \mathbf{p}_i \quad (i = 1, 2, \cdots, n-1)$$
$$a_n = \mathbf{p}_1 - \mathbf{p}_n \quad (7)$$

The straight line passing through the center of gravity and perpendicular to the tipping boundary is $l_i$

$$l_i = (\mathbf{I} - \hat{a}_i \hat{a}_i^{\mathrm{T}}) \mathbf{p}_{i+1} \quad (8)$$

where, $\hat{a}_i = a_i / \|a_i\|$, $\mathbf{I}$ express identity matrix.

The calculation of the edge line tipping angle $\gamma$ can be obtained from the angle between the vertical line $l_i$ of the

**TABLE 3.** Tipping stability angle parameter.

| Configuration | Edge line tipping angle $\gamma/°$ | | | | Corner tipping angles $\Psi/°$ | | | |
|---|---|---|---|---|---|---|---|---|
| | 1 | 2 | 3 | 4 | 1 | 2 | 3 | 4 |
| A | 32.60 | 45.50 | 25.69 | 52.16 | 54.32 | 52.59 | 45.56 | 54.32 |
| B | 32.86 | 51.96 | 25.76 | 52.05 | 53.96 | 52.98 | 54.54 | 54.54 |
| C | 29.32 | 05.34 | 49.92 | \ | 52.25 | 50.79 | 52.25 | \ |

**TABLE 4.** Stability analysis parameter.

| Configuration | Minimum stability angle $\alpha/°$ | Gravity center height $h$/mm | Deflection angle of upper center piece $\theta/°$ |
|---|---|---|---|
| A | 25.69 | 56.45 | 1.91 |
| B | 25.76 | 56.51 | 5.01 |
| C | 5.34 | 59.24 | 4.15 |

tipping axis and the center of gravity vector $f_g$:

$$\gamma_i = \sigma_i \cos^{-1}(\hat{f}_g \hat{l}_i) \quad (i = 1, 2, \cdots, n) \quad (9)$$

$$\sigma_i = \begin{cases} +1, & (\hat{l}_i \times \hat{f}_g) \cdot \hat{a}_i < 0 \\ -1, & \text{others} \end{cases} \quad (10)$$

Similarly, for corner tipping, the corner tipping angle $\psi$ is calculated by the following equation:

$$\psi_i = \varepsilon_i \cos^{-1}(\hat{f}_g \hat{p}_i) \quad (i = 1, 2, \cdots, n) \quad (11)$$

$$\varepsilon_i = \begin{cases} +1, & (\hat{l}_i \times \hat{f}_g) \cdot \hat{a}_i < 0 \text{ or } (\hat{l}_{i+1} \times \hat{f}_g) \cdot \hat{a}_{i+1} < 0 \\ -1, & \text{others} \end{cases} \quad (12)$$

Considering the global stability of the robot:

$$\theta_1 = \min(\gamma_n, \psi_1, \gamma_1)$$
$$\theta_i = \min(\gamma_{i-1}, \psi_i, \gamma_i) \quad (i = 2, \cdots, n) \quad (13)$$

The angle value of the minimum stability angle is:

$$\alpha = \min(\theta_i) \quad (i = 1, \cdots, n) \quad (14)$$

The edge line tipping angle and corner tipping angles of three configurations can be obtained from the above equation as shown in Table 3:

The minimum stability angle $\alpha$ of each configuration in the table is analyzed and compared, and the gravity center height $h$ and the deflection angle $\theta$ of the center piece in the upper layer of each configuration are obtained in the model. The data arrangement is shown in Table 4:

By analyzing the data in the table, it can be concluded from the comparison of the minimum stability angle obtained by the stability pyramid technique that the stability of configuration A and configuration B is far greater than that of configuration C, that is, configuration A and configuration B are less prone to tipping. From the comparison of the height of the center of gravity, it can also be seen that the center of gravity of configuration A and configuration B is lower than that of configuration C, that is, configuration A and configuration B move more stably. Finally, by comparing the
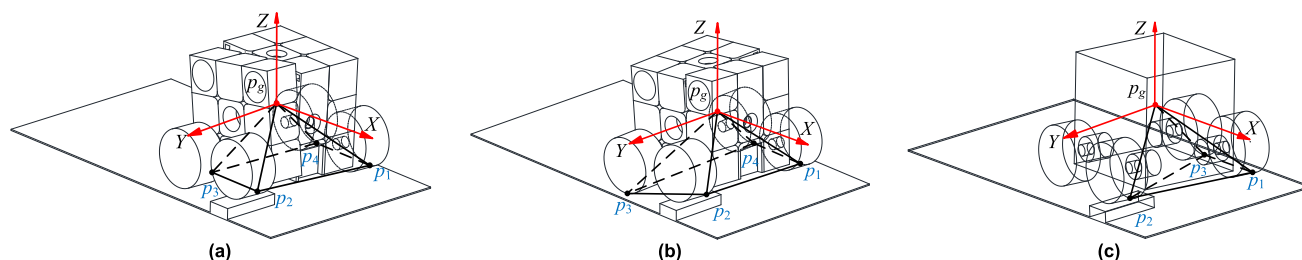
**FIGURE 6.** Stable cone of mobile robot in different configurations. (a) configuration A. (b) configuration B. (c) configuration C.
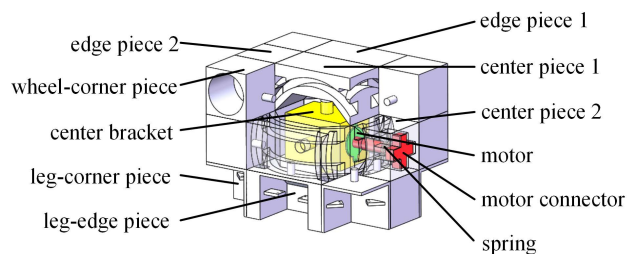


**FIGURE 7.** Wheel-leg conversion module.



**FIGURE 8.** Mechanical leg structure of robot.

deflection angles of upper center piece in three configurations when crossing obstacles, it can be concluded that the deflection angle of configuration A is smaller. Therefore, the selection of configuration A for mobile robot can make the robot have higher stability and obstacle-crossing ability.

## IV. ROBOT DESIGN AND GAIT PLANNING
### A. OVERALL DESIGN OF ROBOT
According to the above configuration selection, the optimized chute third-order RCM is used for the design of the wheel-leg conversion module, and the overall structure of it is shown in Fig. 7. As the torso and core module of the WLMR, it has many basic functions such as connection, support, protection and morphological transformation.

The wheel-leg conversion module consists of corner piece, edge piece, center piece, center bracket, motor, motor connector and spring. The axis of the internal motor output shaft is coincident with the rotation axis of the center piece. The motor is fixed on the central bracket, and its output shaft is connected with the motor connector. The robot can drive the corresponding rotating layer to rotate through the motor to realize the transformation of the robot's wheel form and leg form.

In the wheel-leg conversion module, different cubes adopt different structural designs for mounting wheels and mechanical legs. Among them, four corner pieces on the upper rotating layer are used to install wheels and their driving motors, while four corner pieces and two edge pieces on the lower rotating layer are used to install mechanical legs.

The leg structure of mobile robot is designed based on the leg structure of hexapod, which consists of three joints: basal jo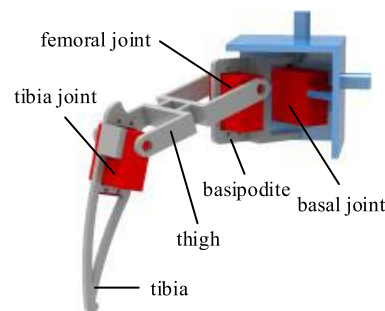int, femoral joint and tibial joint. It has three degrees of freedom, and the structure is shown in Fig. 8. The joints of the mechanical leg are driven by the steering gear, so that the mechanical leg can rotate around three joints, and the overall movement is more flexible. The robot's six mechanical legs have the same structure, and it can realize the road movement in the hexapod form through the coordinated movement of the six mechanical legs.

In the overall structure of mobile robot, there are many kinds of mechanical leg layout schemes. This paper adopts the hexagonal symmetrical layout scheme which is convenient for the robot's motion control, and the hexagonal layout schemes can greatly improve the robot's stability in the motion process and reduce the interference and collision between the legs.

In order to facilitate the mobile robot to move and turn better in wheeled form, the Mecanum wheel is selected as the mobile wheel. Each wheel is controlled by a separate motor, and the robot can realize the gait of moving back and forth, rotating in situ, translating in any direction, etc. in wheeled form through the combination of four Mecanum wheels.

The wheels and mechanical legs are installed on the corresponding cubes of the wheel-leg conversion module, and the wheel-leg mobile robot is constructed. As shown in Fig. 9, its three forms are hexapod, wheel-leg and wheel, respectively. The robot can convert among different forms through the wheel-leg conversion module.

The three forms of mobile robots have different ways of moving. In the wheeled form, the robot can move in any direction in the plane through the control of Mecanum wheels. In the hexapod form, the robot can move on the irregular
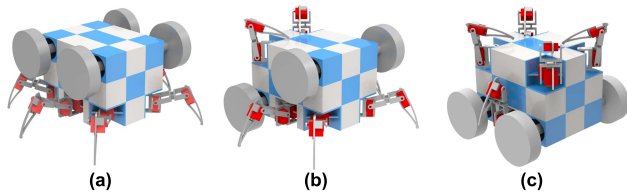
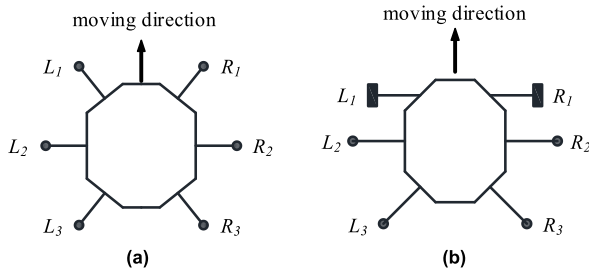**FIGURE 9.** The three forms of the WLMR. (a) hexapod form. (b) wheel-legged form. (c) wheeled form.



**FIGURE 10.** Number of wheels and legs of the mobile robot. (a) hexapod form. (b) wheel-legged form.
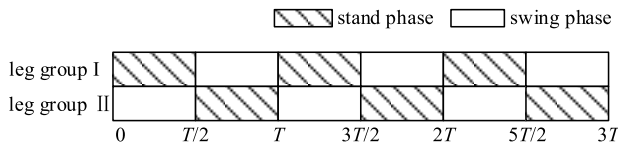


**FIGURE 11.** Three-legged gait phase diagram.



**FIGURE 12.** Three-legged straight gait. (a) I (initial status). (b) I' (the other initial status). (c) $t = 0$ s ($t = $ T). (d) $t = 0$ s ($t = $ T'). (e) $t = $ T/2. (f) $t = $ T'/2. (g) F (final status). (h) F' (the other final status).



**FIGURE 13.** Three-legged rotating gait. (a) I (initial status). (b) I' (the other initial status). (c) $t = 0$ s ($t = $ T). (d) $t = 0$ s ($t = $ T'). (e) $t = $ T/2. (f) $t = $ T'/2. (g) F (final status). (h) F' (the other final status).



**FIGURE 14.** Obstacle-crossing gait of robot in wheel-legged form. (a) I (initial status). (b) $t = 0$ s. (c) $t = $ T/3. (d) $t = $ 2T/3. (e) $t = $ T. (f) F (final status).

road surface by the movement of six mechanical legs. In the wheel-legged form, the robot can achieve obstacle crossing in complex environment through the coordination of the wheel and the mechanical leg, and the robot can make use of the high power of the wheel and the flexibility of the mechanical leg to ensure high stability when crossing obstacles.

### B. GAIT PLANNING
In order to facilitate the analysis, the mechanical legs of the robot in the form of hexapod and wheel-leg are numbered, as shown in Fig. 10. In the hexapod form, mobile robots can move through three-legged gait, four-legged gait and five-legged gait, among which the three-legged gait is widely used because of its good stability. This paper takes the three-legged gait as an example to study the gait planning, and divides the robot's six mechanical legs into two groups: $R_1$, $L_2$ and $R_3$ are leg group I, and $L_1$, $R_2$ and $L_3$ are leg group II.

The gait phase distribution of the robot at any moment is shown in Fig. 11. Two groups of legs alternately support and swing to realize the robot's movement. Its straight gait and in-situ rotation gait are shown in Fig. 12 and Fig. 13 respectively. The foot of the robot is solid when it is in contact with the ground, and the foot is hollow when it is lifted off the ground. In the analysis, the time when the robot switches the support leg is ignored, and the robots before and after the switch are at the same time. The time after the switch is indicated by a special symbol " ' ".
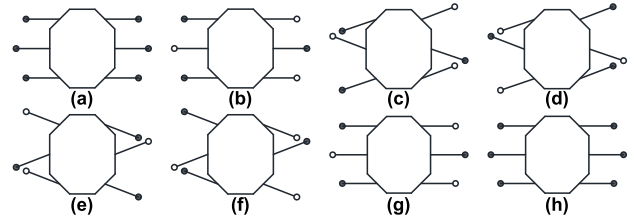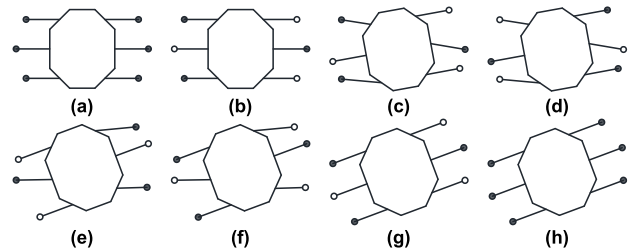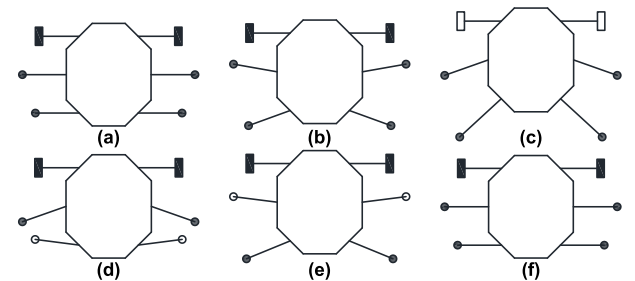
In hexapod form, mobile robot is suitable for most unstructured ground movements, but in some complex environments, hexapod form can't meet the requirements of obstacle-crossing, so the robot needs to be transformed into wheel-legged form. In the wheel-legged form, two wheels of the robot are in contact with the ground, and the two wheels and four mechanical legs realize the robot's obstacle crossing through the alternate conversion of supporting state and swinging state. The robot's mechanical legs are divided into two groups: $L_2$, $R_2$ leg group I, $L_3$, $R_3$ leg group II, and its obstacle-crossing gait diagram is shown in Fig. 14.

The robot can change its form under the action of the wheel-leg conversion module to adapt to different terrains. The robot will lift to a certain height under the action of the mechanical leg in the middle, and the position of the wheels and legs will be exchanged under the action of the motor inside the wheel-legged conversion module.

### C. GAIT STABILITY ANALYSIS
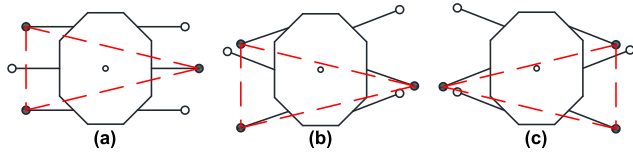Mobile robots often move on unstructured ground and cross obstacles in complex environments, and the gait stability in

**FIGURE 15.** Boundary diagram of gait stability of three-legged straight gait. (a) I′ (the other initial status). (b) $t = 0$ s ($t = T$). (c) $t = T/2$.
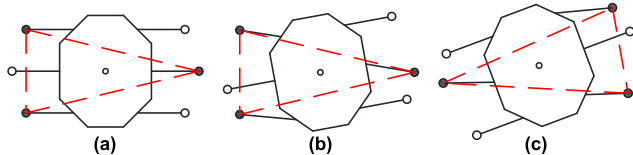


**FIGURE 17.** Boundary diagram of gait stability of wheel-legged obstacle crossing. (a) $t = T/3$. (b) $t = 2T/3$. (c) $t = T$.



**FIGURE 16.** Boundary diagram of gait stability of three-legged rotating gait. (a) I′ (the other initial status). (b) $t = 0$ s ($t = T$). (c) $t = T/2$.

these situations is difficult to guarantee, so the stability analysis of its movement process is a key step. The static stability boundary method [20], one of the static stability analysis methods, is used to analyze these different gait situations.

In the hexapod form, the robot is supported by mechanical legs, and connecting the ends of the supporting legs of the hexapod robot in sequence will form a stable boundary. The stability of the robot is judged by analyzing the situation that the center of gravity of the robot falls within the stable boundary and its distance from the boundary. As shown in Fig. 15, the stability analysis of the robot in the part of the three-legged walking gait shows that its stable boundary is triangular, and the center of gravity of the mobile robot always falls within the stable boundary, so the robot has certain stability in the three-legged gait. When $t = 0$ s or $t = T/2$, the center of gravity of the robot is close to the boundary. At this time, the stability of the robot is low, but it mainly occurs in the extreme position, the overall stability is still high.

Similar to the triangle straight gait, the stable boundary of the triangle rotating gait is triangular, as shown in Fig. 16. It can be seen from the figure that compared with the straight gait, the center of gravity of the rotating gait is far from the boundary and the stability is higher.

The wheel-leg form of mobile robot is mainly used for crossing special obstacles such as steps, and its stability is mainly ensured by the cooperation of mechanical legs and wheels in the process of crossing obstacles. The stability analysis of several key moments in the gait cycle is shown in Fig. 17. When the robot crosses the steps, the worst stability stage is the process in which its four mechanical legs lift the robot wheels. At this time, only four mechanical legs of the robot are in contact with the ground, as shown in Fig. 17(a). And the stability of the robot is poor when the leg group II is lifted up, as shown in Fig. 17(b).

In order to prevent the robot from tipping over during the movement, it is necessary to make a reasonable plan for the obstacle-crossing gait at the above moment to prevent
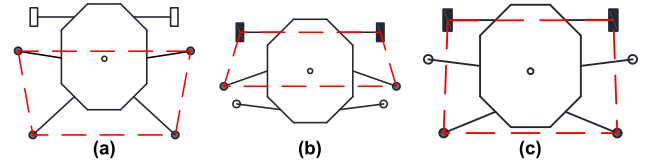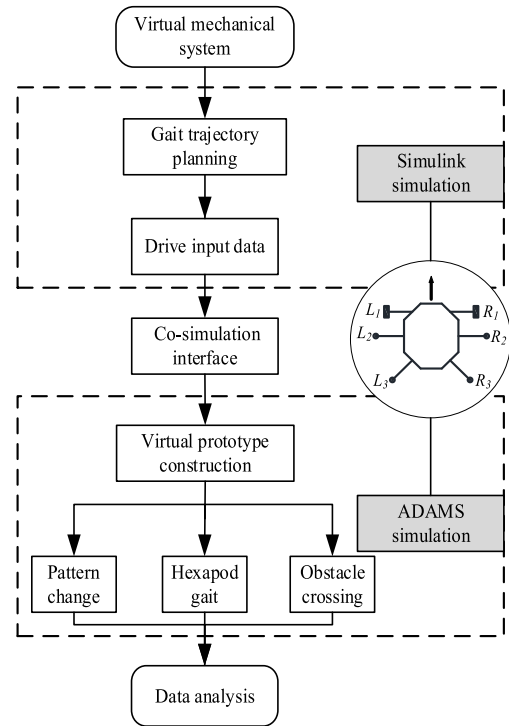


**FIGURE 18.** Co-simulation flow chart.

the center of gravity of the robot from falling outside the stability boundary.

## V. SIMULATION ANALYSIS

Based on the previously planned motion gait, co-simulation experiments were conducted for the straight and rotational motion of the mobile robot under different gait patterns, irregular road movement in the hexapod form and step obstacle crossing in the wheel-legged form, as shown in Fig. 18. The ADAMS virtual mechanical system is imported into the Simulink environment, and 24 rotational state variables are defined as input signals. Finally, the simulation results of the robot are analyzed by measuring the signals of displacement and force during the simulation process.

Morphological transformation is one of the most important functions of the mobile robot, and its transformation simulation process is shown in Fig. 19. It takes the hexapod form as the initial state, as shown in Fig. 19(a). The robot first lifts its front half under the action of two mechanical legs in the middle, and the front rotating layer rotates 180° to exchange the positions of wheel-legs. Then, the wheels are lowered
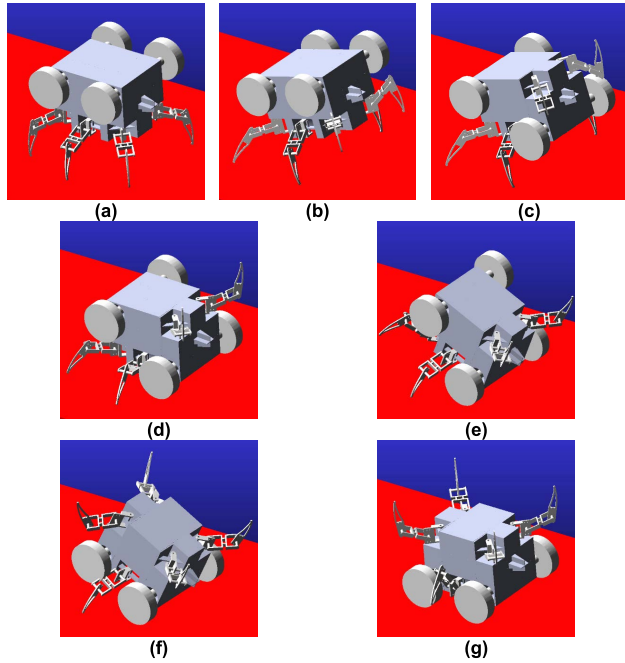
**FIGURE 19.** Simulation of morphological transformation process of mobile robot. (a) $t = 0$ s. (b) $t = 2$ s. (c) $t = 4$ s. (d) $t = 6$ s. (e) $t = 8$ s. (f) $t = 10$ s. (g) $t = 12$ s.



**FIGURE 20.** Variation diagram of gait parameters of mobile robot. (a) The X-axis displacement of the robot in the straight gait. (b) The Y-axis displacement of the robot in the straight gait. (c) The Z-axis displacement of the robot in the straight gait. (d) The angle of the robot in the rotational gait.



**FIGURE 21.** Simulation of the mobile robot in three-legged straight gait. (a) t=0 s. (b) t=2 s. (c) t=4 s.



**FIGURE 22.** Simulation of the mobile robot in three-legged rotational gait. (a) t=0 s. (b) t=2 s. (c) t=4 s. (d) t=6 s. (e) t=8 s. (f) t=10 s.

to contact the ground through the mechanical legs, and the robot is transformed into the wheel-legged form, as shown in Fig. 19(d).

Similarly, the robot can also be converted from the wheel-legged form to the wheeled form in a similar process as described above, with the final form shown in Fig. 19(g). Conversely, the robot can be converted from the wheeled form to the hexapod form.

In the hexapod form, the robot can achieve a variety of mobile gaits to adapt to different terrains through the cooperation of six mechanical legs. The motion of the robot in each gait is simulated in ADAMS, and the duration of one step of the mechanical leg is set to 2 s. The rotation speed of the base joint of the mechanical leg is set to 0.4 r/s. The displacement of the robot in the three-legged gait (3L gait), four-legged gait (4L gait), and five-legged gait (5L gait) while walking straight or rotating in place are shown in Fig. 20.

The mobile robot is faster than other gaits when it moves straight or rotates in place under the three-legged gait, and the displacement fluctuation along the Z-axis direction is no more than 1 mm, as shown in Fig. 20(c). Therefore, the robot chooses the three-legged gait as its main application gait in the movement process, and the simulation of its straight and rotational gait is shown in Fig. 21 and Fig. 22. The simulation shows that the robot can successfully achieve the straight and rotational motion, and the change of displacement in each direction during the motion process is small, so the robot has good stability.

Step climbing, as a classic obstacle, has always been one of the difficulties for mobile robots to overcome. The mobile
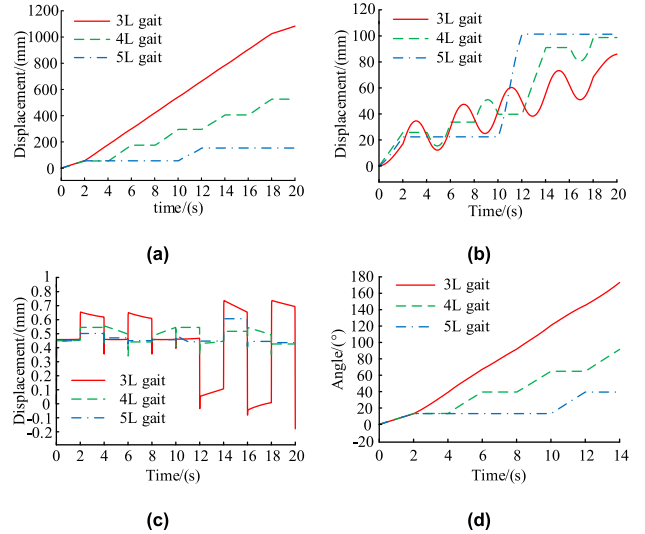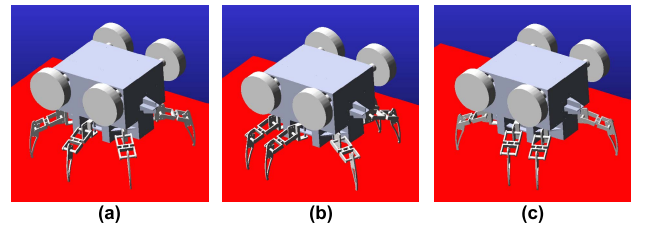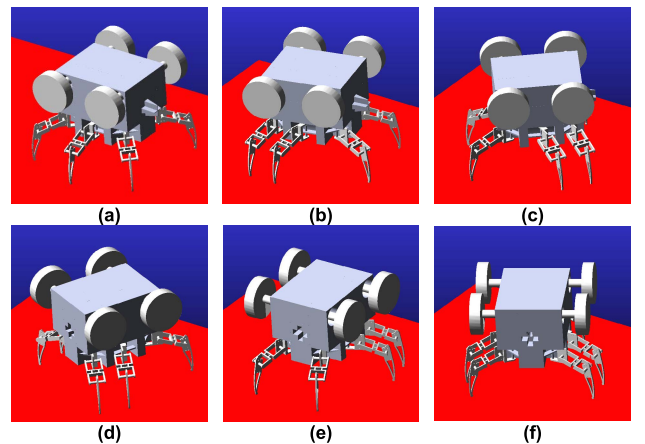
robot proposed in this paper can achieve a more stable and efficient obstacle crossing by planning its gait of climbing steps in wheel-legged form.

The simulation diagram of the obstacle crossing process is shown in Fig. 23. The robot first props up the two wheels at
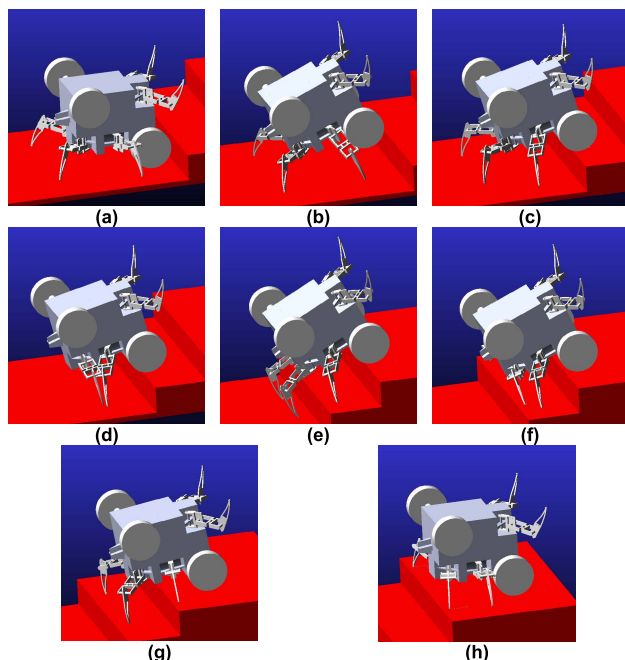
**FIGURE 23.** Simulation of the mobile robot in wheel-legged and obstacle-crossing gait. (a) t=0 s. (b) t=2 s. (c) t=4 s. (d) t=6 s. (e) t=8 s. (f) t=10 s. (g) t=12 s. (h) t=14 s.

the front through the two mechanical legs in the middle, and the four mechanical legs turn backward at the same time to send the wheels to the first step, as shown in Fig. 23(c); then the robot moves forward with the cooperation of the wheels and the rear mechanical legs, while the two mechanical legs in the middle step up the first step, and send the wheels to the second step through a similar gait process as described before, as shown in Fig. 23(e); by continuously cycling the previous gait, the robot can finally achieve step climbing. During the step crossing process of the robot, the friction between the wheels and the ground is used to provide power to move the robot forward, which fully reflects the advantages of the robot in the wheel-legged form.

## VI. EXPERIMENTAL VERIFICATION

By optimizing the structure and appearance of the robot, an experimental prototype was developed. In order to facilitate the experimental analysis, the lateral rotation of the robot is cancelled. At this time, the front and rear rotation layers of the wheel-leg conversion module can normally rotate to convert the wheeled and legged form.

This mobile robot prototype mainly includes several basic parts such as power module, control system, drive unit and body structure. As for the specific driving implementation, the steering gear is used as the driver of the mechanical leg joint and the wheel-leg conversion module, and the DC motor is used as the driver of the Mecanum wheel. The prototype of the mobile robot is shown in Fig. 24, and its parameters are shown in Table 5.
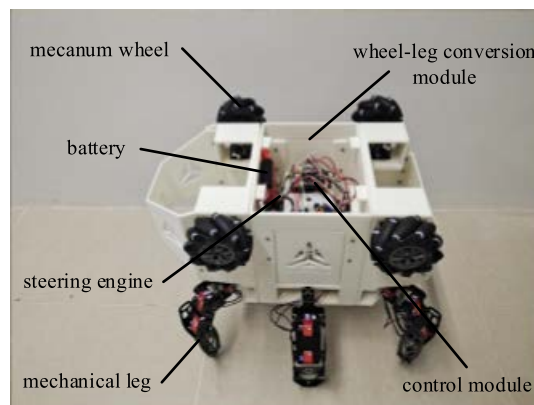


**FIGURE 24.** Structure diagram of mobile robot prototype.

**TABLE 5.** Parameter table of mobile robot prototype.

| Prototype | Parameter |
|---|---|
| Weight | 4 kg |
| Fuselage material | Synthetic resin |
| Leg material | Aluminium alloy |
| Leg steering gear model | 20 kg bus steering gear |
| Wheel-legged conversion module Steering gear model | 60 kg PWM steering gear |
| Operating voltage | 6.8 V |



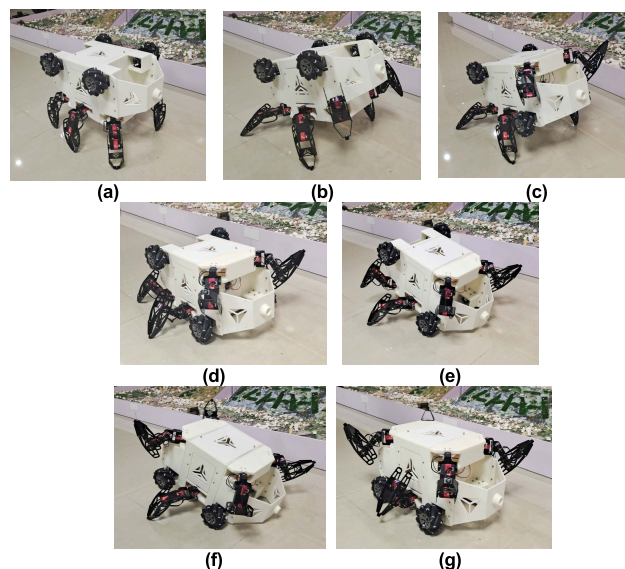**FIGURE 25.** Morphological transformation experiment of the robot. (a) t=0 s. (b) t=2 s. (c) t=4 s. (d) t=6 s. (e) t=8 s. (f) t=10 s. (g) t=12 s.

The mobile robot has three iforms, and different forms can adapt to different terrain. The feasibility of its form conversion function can be proved by the prototype experiment.

Three forms of the prototype and the transformation process are shown in Fig. 25, and the process is consistent with the simulation results. Fig. 25(a), Fig. 25(d) and Fig. 25(g)
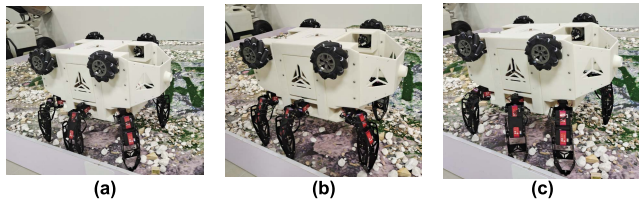
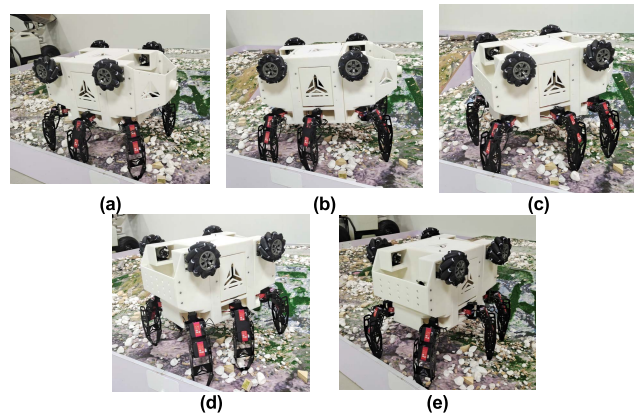**FIGURE 26.** Straight gait experiment of robot in hexapod form. (a) t=0 s. (b) t=2 s. (c) t=4 s.



**FIGURE 27.** Rotating gait experiment of robot in hexapod form. (a) t=0 s. (b) t=2 s. (c) t=4 s. (d) t=6 s. (e) t=8 s.



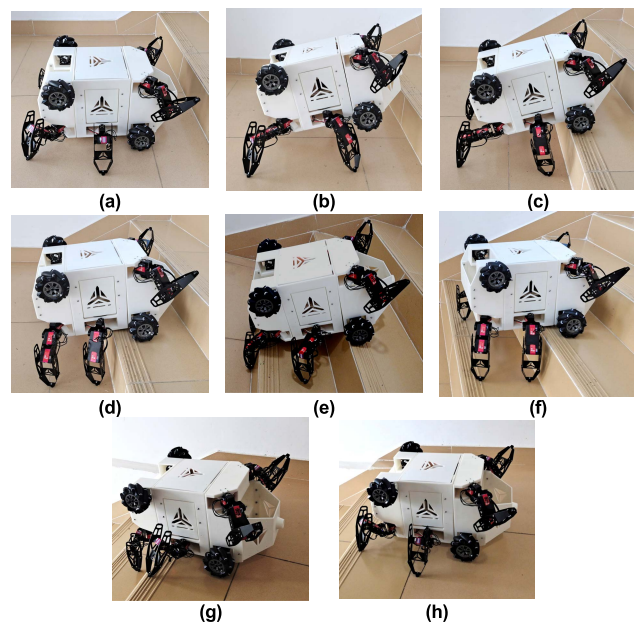**FIGURE 28.** Obstacle-crossing experiment of robot in the wheel-legged form. (a) t=0 s. (b) t=2 s. (c) t=4 s. (d) t=6 s. (e) t=8 s. (f) t=10 s. (g) t=12 s. (h) t=14 s.

are hexapod form, wheel-legged form and wheeled form respectively in this figure.

Experiments were carried out on the three-legged walking and rotating gait of the robot prototype in the hexapod form, and the processes are shown in Fig. 26 and Fig. 27 respectively. The robot can go straight and turn normally on the

unstructured ground covered with stones, and its movement process is consistent with the simulation results.

Finally, the experiment of the robot climbing the steps in the form of wheels and legs is carried out, as shown in Fig. 28. The experiment shows that the robot can successfully achieve obstacle-crossing with a height of 120 mm.

## VII. CONCLUSION

(1) In order to improve the obstacle-crossing ability, motion stability and load-bearing capacity of mobile robots for different terrains, the RCM with strong coupling and variable topology is introduced into the field of mobile robots, and a WLMR based on RCM is proposed.

(2) By optimizing the rotation mode of the classic third-order RCM, a new type of chute third-order RCM is designed, and the advantages of the new mechanism in daily production and life are verified through the analysis of force characteristics and feasibility.

(3) Based on the flexible and variable metamorphic properties of the RCM, a driving configuration analysis method is established according to different driving configuration relationships A total of 64 configurations are synthesized, and the final configuration of the WLMR is determined through configuration stability analysis. The morphology transformation function and high adaptability of the mobile robot are realized.

(4) A WLMR with polymorphism is constructed by combining wheel-leg conversion module, mechanical leg and Mecanum wheel. The gait planning and gait stability analysis are carried out for it, which ensures the motion stability of various gaits.

(5) The co-simulation and prototype experiments are performed to verify the efficiency of the WLMR's straight motion, in-situ rotation, obstacle-crossing and morphology transformation in complex environments. This research not only provides a reference for the design of polymorphous mobile robots, but also opens up ideas for the application of the RCM in daily production and life.

Although this study has improved the self-adaptability of WLMR in different environments to some extent, it is still lacking in environmental perception and intelligent decision-making. In the follow-up, the adaptive control research based on this polymorphic mobile robot will be carried out.

## REFERENCES

[1] A. Vijaychandra, C. Alex, M. Mathews, and A. A. Sathar, "Amphibious wheels with a passive slip mechanism for transformation," in *Proc. IEEE 4th Int. Conf. Adv. Robot. Mechatronics (ICARM)*, Jul. 2019, pp. 960–965.

[2] X. Ding, K. Li, and K. Xu, "Dynamics and wheel's slip ratio of a wheel-legged robot in wheeled motion considering the change of height," *Chin. J. Mech. Eng.*, vol. 25, no. 5, pp. 1060–1067, Sep. 2012.

[3] X. L. Ding and K. Xu, "Design and analysis of a novel metamorphic wheel-legged rover mechanism," *J. Central South Univ., Sci. Technol.*, vol. 40, pp. 91–101, 2009.

[4] M. Bjelonic, P. K. Sankar, C. D. Bellicoso, H. Vallery, and M. Hutter, "Rolling in the deep—Hybrid locomotion for wheeled-legged robots using online trajectory optimization," *IEEE Robot. Autom. Lett.*, vol. 5, no. 2, pp. 3626–3633, Apr. 2020.

[5] Y. Morihiro, N. Takahashi, K. Nonaka, and K. Sekiguchi, "Model predictive load distribution control for leg/wheel mobile robots on rough terrain," *IFAC-PapersOnLine*, vol. 51, no. 22, pp. 441–446, 2018.

[6] Z. H. Chen, S. K. Wang, J. Z. Wang, K. Xu, X. W. Wang, D. H. Liu, T. Lei, and J. G. Si, "Motion drive and multi-mode control method of an electric parallel six wheel-legged robot," *Robot*, vol. 42, no. 5, pp. 534–549, 2020.

[7] X. W. Wang, S. K. Wang, J. Z. Wang, Z. H. Chen, K. Xu, and D. H. Liu, "Electric parallel hexapod robot based on special-shaped Stewart platform," *J. Mech. Eng.*, vol. 56, no. 13, pp. 84–92, 2020.

[8] S. Nakajima, E. Nakano, and T. Takahashi, "Motion control technique for practical use of a leg-wheel robot on unknown outdoor rough terrains," in *Proc. IEEE/RSJ Int. Conf. Intell. Robots Syst. (IROS)*, Sep. 2004, pp. 1353–1358.

[9] C. Y. Zhang, S. Guo, and F. Q. Zhao, "Motion analysis and gait research of a new wheel-legged compound robot," *J. Mech. Eng.*, vol. 55, no. 15, pp. 145–153, 2019.

[10] S.-C. Chen, K.-J. Huang, W.-H. Chen, S.-Y. Shen, C.-H. Li, and P.-C. Lin, "Quattroped: A leg-wheel transformable robot," *IEEE/ASME Trans. Mechatronics*, vol. 19, no. 2, pp. 730–742, Apr. 2014.

[11] W.-H. Chen, H.-S. Lin, Y.-M. Lin, and P.-C. Lin, "TurboQuad: A novel leg–wheel transformable robot with smooth and fast behavioral transitions," *IEEE Trans. Robot.*, vol. 33, no. 5, pp. 1025–1040, Oct. 2017.

[12] F. Zhou, H. Xu, T. Zou, and X. Zhang, "A wheel-track-Leg hybrid locomotion mechanism based on transformable rims," in *Proc. IEEE Int. Conf. Adv. Intell. Mechatronics (AIM)*, Jul. 2017, pp. 315–320.

[13] J. S. Dai and D. Wang, "Geometric analysis and synthesis of the metamorphic robotic hand," *J. Mech. Des.*, vol. 129, no. 11, pp. 1191–1197, Nov. 2007.

[14] W. K. Zhen, X. Kang, X. S. Zhang, and J. S. Dai, "Gait planning of a new quadruped metamorphic crawling robot," *J. Mech. Eng.*, vol. 52, no. 11, pp. 26–33, 2016.

[15] C. Liu, X. C. Tan, Y. A. Yao, and Z. Y. Fu, "Design and analysis of a novel deformable wheel-legged robot," *J. Mech. Eng.*, vol. 58, no. 3, pp. 65–74, 2022.

[16] D.-X. Zeng, M. Li, J.-J. Wang, Y.-L. Hou, W.-J. Lu, and Z. Huang, "Overview of Rubik's cube and reflections on its application in mechanism," *Chin. J. Mech. Eng.*, vol. 31, no. 1, pp. 9–20, Dec. 2018.

[17] D. Zeng, M. Li, J. Wang, S. Sun, X. Luo, Y. Hou, W. Lu, and Z. Huang, "Analysis of structural composition and representation of topological structures of Rubik's cube mechanism," *Mechanism Mach. Theory*, vol. 136, pp. 86–104, Jun. 2019.

[18] W. J. Lu, H. F. Wu, T. L. Liu, and D. X. Zeng, "Topology and motion diagram of the third-order cube mechanism," *J. Mech. Eng.*, vol. 56, no. 23, pp. 89–97, 2020.

[19] B. Li, J. G. Liu, and D. L. Tan, "Research on the tipover stability of a reconfigurable modular robot," *Robot*, vol. 27, no. 3, pp. 241–246, 2005.

[20] R. B. Mcghee and G. I. Iswandhi, "Adaptive locomotion of a multilegged robot over rough terrain," *IEEE Trans. Syst., Man, Cybern.*, vol. SMC-9, no. 4, pp. 176–182, Apr. 1979.

**SHIHAO DONG** is currently pursuing the degree with the School of Mechanical Engineering, Yanshan University. His research interests include metamorphic mechanism and its application.

**DABAO FAN** is currently pursuing the Ph.D. degree with the School of Mechanical Engineering, Yanshan University. His main research interests include parallel mechanism, reconfigurable mechanism, and synthesis of the mechanism.
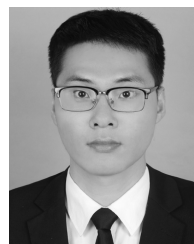
**YA LIU** is currently pursuing the Ph.D. degree with the School of Mechanical Engineering, Yanshan University. His research interests include theory of mechanism and machine, parallel mechanism, and type synthesis.

**DAXING ZENG** was born in 1978. He received the Ph.D. degree in mechatronic engineering from Yanshan University, in 2008. He is currently a Professor at the Dongguan University of Technology, China. His research interests include theory of mechanism and machine, parallel mechanism, type synthesis, and image processing.
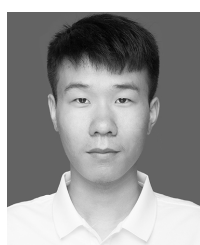
**WENJUAN LU** was born in 1983. She received the Ph.D. degree in mechatronic engineering from Yanshan University, in 2015. She is currently an Associate Professor at the Dongguan University of Technology, China. Her research interests include parallel mechanism and type synthesis.

**JIAHAO ZENG** is currently pursuing the degree with the School of Mechanical Engineering, Yanshan University. His research interests include theory of mechanism and machine, parallel mechanism, and type synthesis.

**MIAOYAN CAO** was born in Hunan, China, in 1978. He received the B.S. degree in mechatronics engineering and the Ph.D. degree in mechanical design and theory from Yanshan University, Qinhuangdao, China, in 2001 and 2012, respectively. He is currently a Professor at the Yanshan University, China. His research interests include ultrasonic assisted forming of tube/sheet metal and light alloy forming process.

● ● ●